Supporting Information

Element Doping-Driven Band Regulation toward Stable 4.5 V Sodium-Ion Layered Oxides

Keyu Pan†[1], Hailong Yang†[1], Xiufang Zheng[1], Binwei Zhang[1]*, Baodan Zhang[1]*

[1] Center of Advanced Electrochemical Energy, Institute of Advanced Interdisciplinary Studies, School of Chemistry and Chemical Engineering, Chongqing University, Chongqing 401331, China

* Correspondence to: zbd@cqu.edu.cn (B. Z.)

KEYWORDS: substitution/doping, TM-O bond, anionic redox, high-voltage, sodium-ion layered oxides cathodes

Experimental Section

Materials synthesis:

The P2-$Na_{0.67}Ni_{0.33-x}Zn_xMn_{0.67}O_2$ materials (x = 0.02, 0.05, 0.08, 0.10, and 0.12 donated as NNMO, NNZMO) were prepared by a simple solid-state synthesis method. The amount of Zn doping is optimized (Fig. 3). Thus, the NNZMO is selected for further investigation. In a typical synthesis of NNZMO, stoichiometric amounts of Na_2CO_3 (5% excess, Aladdin, 99.0%), MnO_2 (Aladdin, 99.0%), ZnO (Aladdin, 99.0%), and NiO (Aladdin, 99.0%) were uniformly mixed using a high-energy ball mill. The powders were calcined at 900 °C for 15 h in a muffle furnace in air with a ramping rate of 5 °C/min and cooled to room temperature naturally. The NNMO was synthesized by a similar process without and ZnO.

Material characterization:

The phase structure of the material was measured by powder X-ray diffraction patterns (XRD, D8 Bruker Advance) with Cu Ka radiation (k = 0.15406 nm) in the scan range (2h) of 5°-90°. The XRD Rietveld refinement was conducted by Fullprof software. The scanning electron microscopy (SEM, Quanta FEG 250) was employed to observe the morphology of the prepared samples. The transmission electron microscope (TEM, JEM-F200, JEOL) and energy dispersive X-ray energy

spectroscopy (EDS) were employed to further collect detailed structural information and the elements distribution. The chemical composition of the prepared materials was tested by inductively coupled plasma-atomic emission spectroscopy (ICP-MS). Xray photoelectron spectroscopic (XPS, Thermo Fisher-K-Alpha, UK) measurement was used to characterize the chemical valence states of material elements.

Electrochemical measurements:

The working electrodes were made by active material (80 wt%), acetylene black (10 wt%), and poly (vinylidene fluoride) (PVDF, 10 wt%) on an aluminum foil. CR2032 coin-type cells were assembled in an argon-filled glove box (Mikrouna Universal 2440/750). The electrolyte is 1 M $NaPF_6$ in DMC : EC = 1 vol% with 5 vol% FEC. The galvanostatic charge/discharge performance was evaluated on a Neware battery testing system (MHW200) in the voltage range of 2.0-4.5 V (1 C refers to 100 mA g^{-1}). Electro-chemical impedance spectra (EIS) were obtained using the VersaSTAT 4 electrochemical workstation. All the electrochemical tests were carried out at room temperature.

Computational details:

A bulk phase of $Na_{12}Ni_6Mn_{12}O_{36}$ was constructed to simulate the P2-$Na_{2/3}Ni_{1/3}Mn_{2/3}O_2$ system. To determine the detailed positions of Zn doping in layered NNMO, we simulated Zn-doped constructing $Na_{11}Ni_6Zn_1Mn_{12}O_{36}$ (NNZMO-0.1Na), $Na_{12}Ni_5Zn_1Mn_{12}O_{36}$ (NNZMO-0.1Ni) models, corresponding to the replacement Na or Ni sites. The first-principles calculations were performed using Density Functional Theory (DFT) and the Vienna Ab initio Simulation Package (VASP). [1] The calculations were based on the Generalized Gradient Approximation (GGA) using the Perdew-Burke-Ernzerhof (PBE) [2] functional. The Grimme's DFT-D3 method [3] with the zero damping function was used to integrate van der Waals interactions. The plane-wave cutoff energy was set to 500 eV and a 3 × 3 × 2 k mesh was applied, and the convergence criteria for the energy and force in the structural optimization process were 10^{-5} eV and 0.03 eV/Å, respectively. To enhance the computational accuracy, the Hubbard U parameters for transition metals were considered, with the Hubbard U values chosen as 7.5 eV for Zn, [4] 3.4 eV for Ni, [5] 4.0 eV for Fe, and 4.0 eV for

Mn. [6]

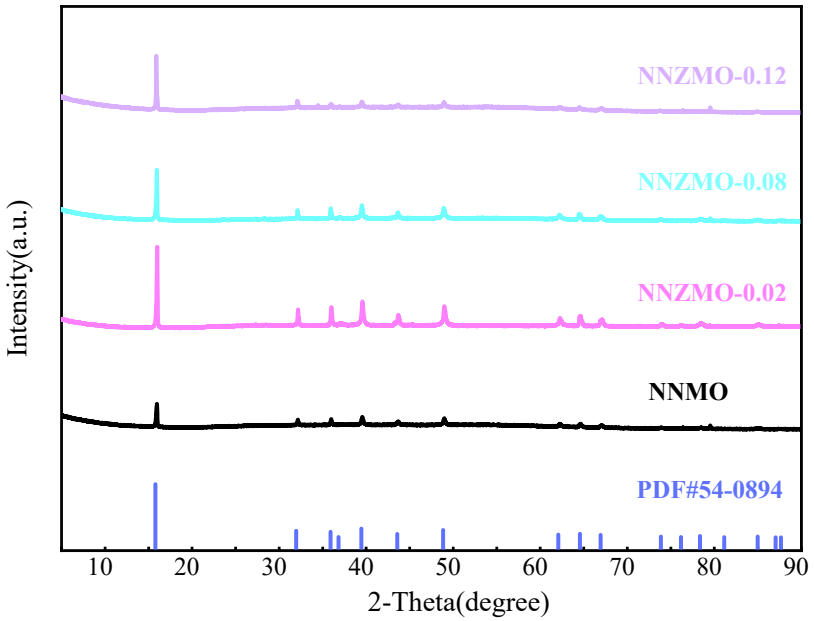

Figure. S1 XRD patterns of NNMO, NNZMO-0.05, NNZMO-0.08, NNZMO-0.10, NNZMO-0.12

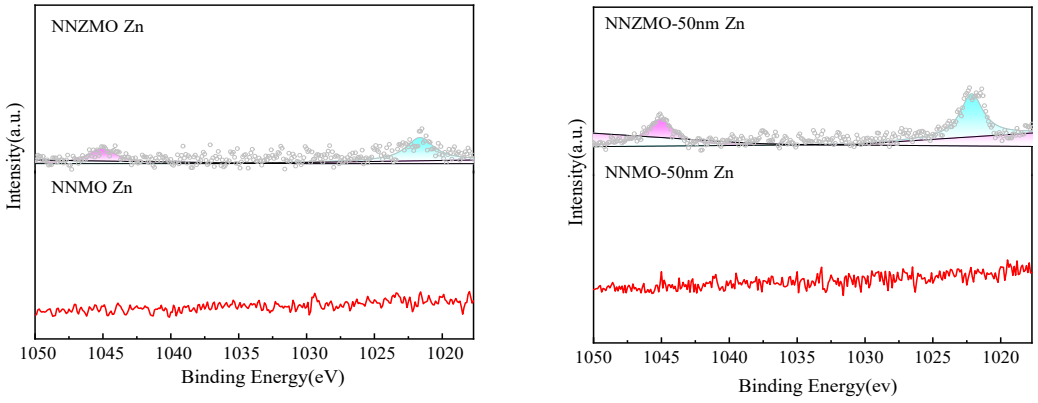

Figure. S2 Zn 2p XPS spectra collectedform the (a) NNMO, NNZMO unetched surface and NNMO, NNZMO etching to a depth of 50 nm cathodes.

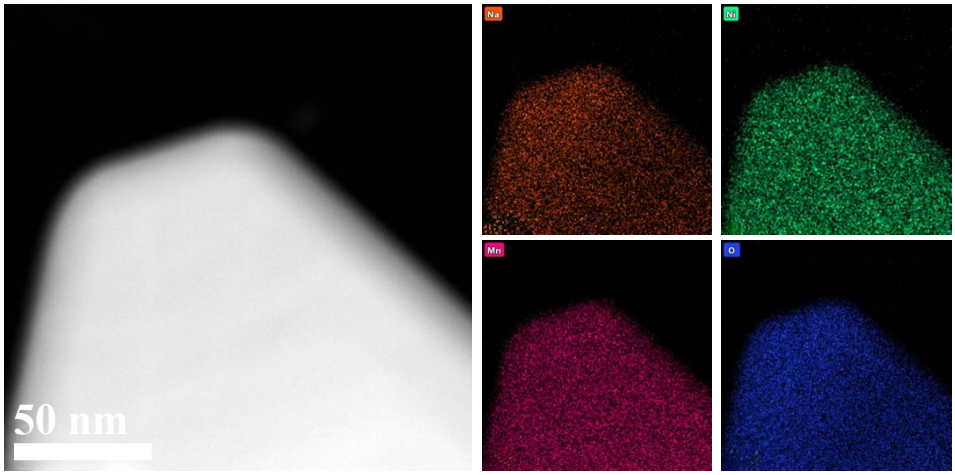

Figure. S3 EDS mapping images of NNZMO.

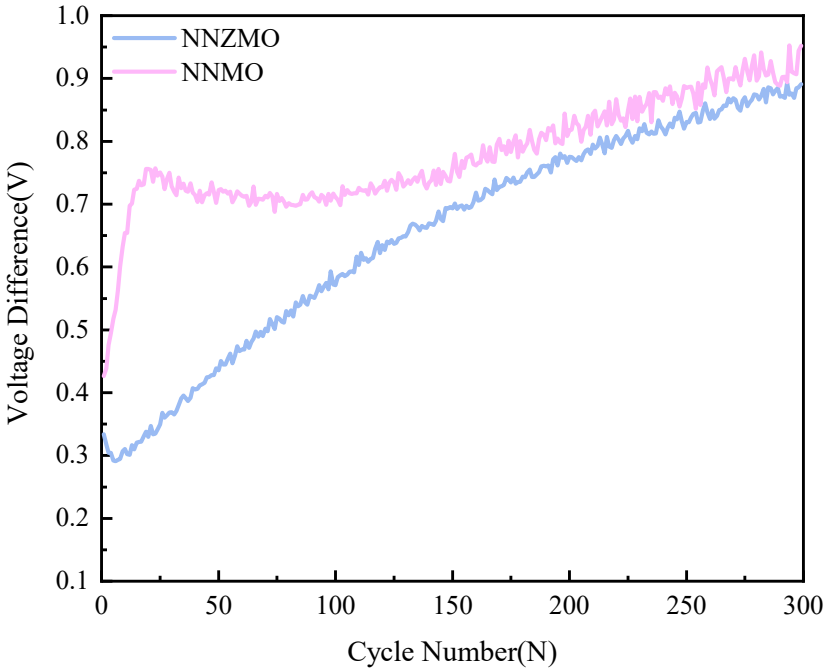

Figure. S4 The average voltage difference between NNMO and NNZMO during 300 cycles at 2C.

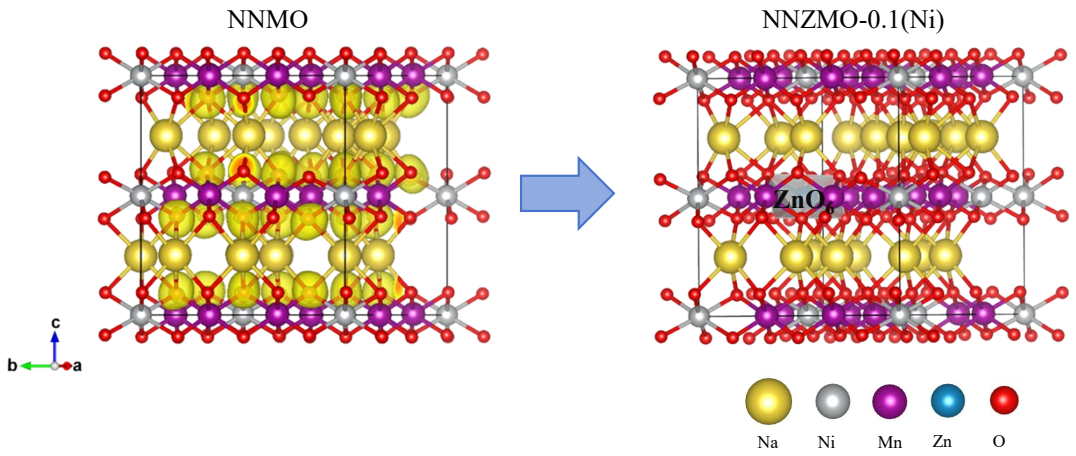

Figure. S5 The electron density map of (a) NNMO and (b) NNZMO

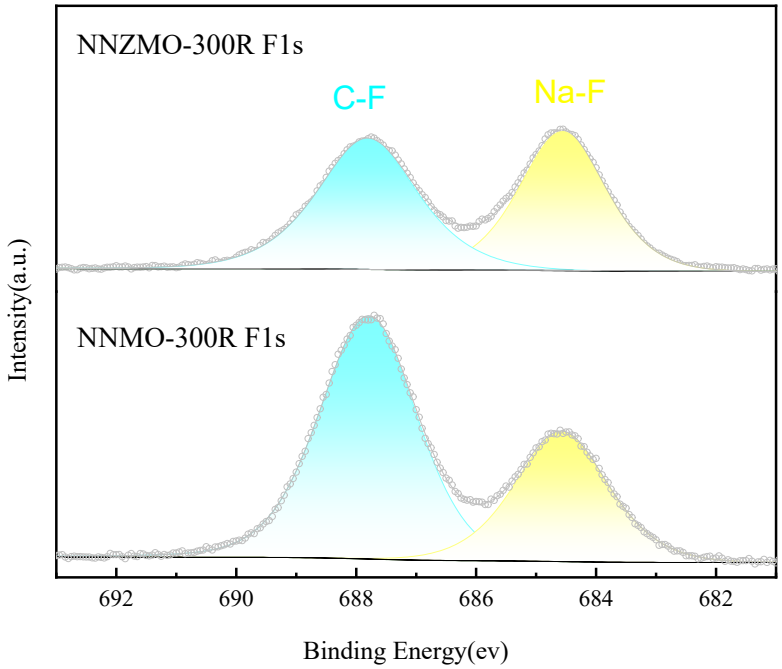

Figure. S6 F1s XPS spectra collected form the NNMO, NNZMO etching to a depth of 50 nm cathodes after 300 cycles.

Table S1 ICP-OES results of NNZMO sample.

Sample	Test Element	W(%)	n(%)
NNZMO	Mn	35.7518%	65.07671884
NNZMO	Na	14.2030%	61.75220444
NNZMO	Ni	13.6681%	23.28863499
NNZMO	Zn	6.2143%	9.503477408

Table S2 Crystallographic details of NNMO and NNZMO obtained from Rietveld analysis.

Sample	Phase	*a* (Å)	*b* (Å)	*c* (Å)	*V* (Å^3)
NNMO	P63/mmc	2.88772	2.88772	11.16324	80.618
NNZMO	P63/mmc	2.88995	2.88995	11.16403	80.748

Table S3. Bader charge of the O atoms analysis of NNMO and NNZMO in the Ni/MnO_6

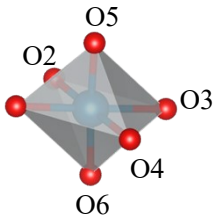

NNMO	Bader charge/e	NNZMO	Bader charge/e
O1	-0.9722	O1	-1.0633
O2	-1.0464	O2	-1.0951
O3	-0.9960	O3	-1.0303
O4	-0.8857	O4	-0.9748
O5	-0.9872	O5	-1.0632
O6	-0.9556	O6	-0.9917
Average	-0.9738	Average	-1.0364

Table S4. The Rs, Rcei, Rct value of the electrode at different cycle number.

	NNMO			NNZMO		
Cycle Number(N)	Rs (Ω)	Rcei (Ω)	Rct (Ω)	Rs (Ω)	Rcei (Ω)	Rct (Ω)
3	1.807	9928	2251	1.789	6553	1236
10	1.822	2058	6982	1.699	611.1	6477
30	3.729	894.9	2697	1.987	337.1	1380

References

[1] Kresse, G.; Furthmüller, J., Efficiency of ab−initio Total Energy Calculations for Metalsand Semiconductors Using a Plane−Wave Basis Set. *Phys. Rev. B*, **1996**, *54*, 11169−11186.

[2] Perdew, J. P.; Burke, K.; Ernzerhof, M., Generalized Gradient Approximati on Made Simple. *Phys. Rev. Lett*., **1996**, *77*, 3865−3868.

[3] Grimme, S.; Antony, J.; Ehrlich, S.; Krieg, H., A Consistent and Accurate Ab Initio Parametrization of Density Functional Dispersion Correction (DFT−D) for the 94 Elements H−Pu. *J. Chem. Phys*., **2010**, *132*, 154104.

[4] Erhart, P., Albe, K. & Klein, A. First-principles study of intrinsic point def ects in ZnO: Role of band structure, volume relaxation, and finite-size effects. *Phys. Rev. B* **73**, 205203 (2006).

[5] Anisimov, V. V., Zaanen, J. & Andersen, O. K. Band theory and Mott ins ulators: Hubbard U instead of Stoner I. *Phys. Rev. B Condens. Matter.* **44**, 943 -954 (1991).

[6] Wang, L., Maxisch, T. & Ceder, G. Oxidation energies of transition metal oxides within the GGA+U framework. *Phys. Rev. B* **73**, 195107 (2006).